

Simulation of Eddy-Current Separators

P. C. Rem, E. M. Beunder, and A. J. van den Akker

Abstract—A model is presented for the simulation of rotary drum eddy-current separators. The most important part of the model is an improved first-order differential equation for the magnetic moment of nonferrous particles in the field of the separator magnets. The model also includes the mechanical interaction between the particles and the transportation belt, as well as aerodynamic forces. The resulting particle trajectories are compared to experimental data, both on the basis of full trajectories and statistically, in terms of the calculated and measured throw.

Index Terms—Eddy current, model, nonferrous.

I. INTRODUCTION

EDDY CURRENT separation is an effective way of recovering nonferrous metals from streams of industrial or municipal waste [1]. The process is used to separate aluminum and copper from car scrap and to remove metals from recycle glass. The separation is brought about by inducing eddy currents inside the conductive particles of the stream. These currents lend a magnetic moment to the particles which are then propelled by the gradient field of the magnets [2]. Today, the rotary drum is the most widely used type of eddy current separator. The active part of this machine is a fast spinning drum, with a surface consisting of rows of magnets of alternating polarity (see Fig. 1). A conveyor belt takes the particles over the drum and the conductive particles are accelerated so as to follow the motion of the drum. Poorly conducting materials, on the other hand, will stay on the belt and drop close to the drum. The trajectory of particles is generally determined by a combination of the electromotive force, gravity, and the forces of the conveyor belt and the air.

The modeling of the interaction between the magnetic field and conductive particles is complicated by the existence of three characteristic sizes: the particle size, the pole width or magnetic wavelength of the separator, and the skin depth. For materials with high conductivities, such as aluminum and copper, three size regimes can be distinguished: large particles of a size exceeding about one third of the wavelength of the field, medium sized particles which are small enough to neglect spatial variations of the magnetic field gradient over the volume of the particle yet large enough to shield the field from their interior, and small particles that are penetrated by the field.

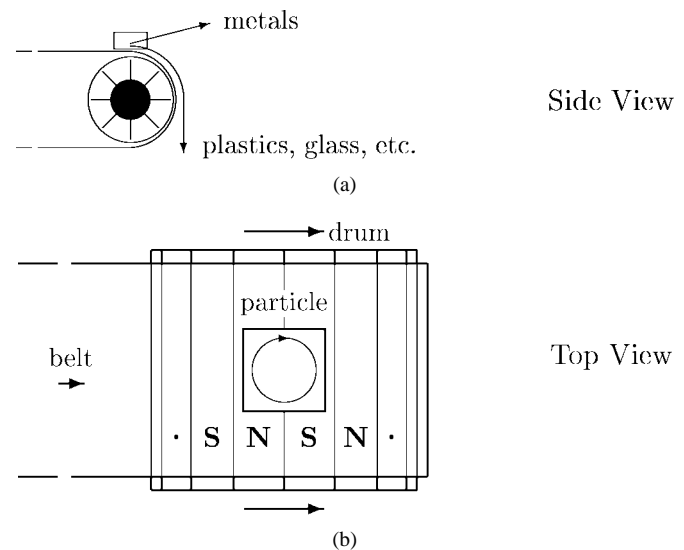


Fig. 1. An eddy current separator consists of a drum covered with magnets that are oriented alternately N-S and S-N. The fluctuating field of the spinning drum induces eddy currents in electrically conductive particles moving close to the drum. The particles are then expelled along the direction of rotation. (a) The pictures show an eddy current separator as viewed from aside and (b) from above.

Most of the theory developed before the 1990's, in particular the work by Schlömann [3], [4] and van der Valk *et al.* [5]–[7], is dealing with the limit of small particles or low frequencies, although this is not always clearly stated. It is also often assumed, for simplicity, that the electromagnetic interaction is not affected by the rotational motion of the particle. This assumption is generally correct for symmetric fields, i.e., fields generated by two symmetric faces of magnets. However, for asymmetric fields such as in the rotary drum designs, spinning of the particles reduces the separation forces, especially for small particles. In the early 1990's, work was done on larger particles by Fletcher *et al.* [9]–[11] starting from first principles. The results of this model show a fair correspondence with experimental results. However, both particle and field geometry were different from what is common in practical applications. Recently, Meier-Staude *et al.* [8] simulated a rotary drum including the conveyor belt. This model does not contain a radial component of the magnetic force and the particle shape is uncommon.

The present model was developed by treating the particles as magnetic dipoles [12], [13]. This model can cope with small and medium-sized particles in both symmetric and asymmetric fields. It will be presented in the next section, together with the model for the mechanical interactions. The remainder of the paper will deal with the experimental verification of the model.

Manuscript received February 24, 1998; revised March 30, 1998.

The authors are with Delft University of Technology, 2628 RX Delft, The Netherlands (e-mail: p.c.rem@ta.tudelft.nl; e.m.beunder@ta.tudelft.nl; w.kuilman@ta.tudelft.nl).

Publisher Item Identifier S 0018-9464(98)04315-5.

II. THE DIPOLE MODEL

Provided that variations of the field gradient $\nabla \mathbf{B}^a$ within the particle are sufficiently small, the force \mathbf{F} of an external magnetic field \mathbf{B}^a on a particle can be expressed in terms of its magnetic moment \mathbf{M} [14]

$$\mathbf{F} = \mathbf{M} \cdot \nabla \mathbf{B}^a = M_x \nabla B_x^a + M_y \nabla B_y^a + M_z \nabla B_z^a. \quad (1)$$

Similarly, the torque on the particle is then given by

$$\mathbf{T} = \mathbf{M} \times \mathbf{B}^a. \quad (2)$$

In relation to eddy current separators, the above approximation is sufficiently accurate if the particles are smaller than about one third of the wavelength of the magnetic field (or equivalently, one third of the width of a pair of magnetic poles). This means that for rotary drum machines, the model is limited to particles with diameters less than 30 to 50 mm, depending on the number of poles. Fortunately, this is the more interesting size range from a technological point of view, since larger nonferrous particles are easily separated from nonmetals and the resulting product is usually sorted by hand or color sensors.

Once the dipole approximation is accepted, the problem of computing the electromotive forces reduces to the computation of the field of the separator and the magnetic moment of the particle. It turns out that the latter can be done most easily in a coordinate frame that is moving and co-rotating with the particle. In this frame, \mathbf{M} can be related to \mathbf{B}^a by a simple first order differential equation [12], [13].

A. Separator Magnetic Field

The first step in computing the field as observed by a moving particle is to express the field generated by the magnets of the eddy current separator as a function of the coordinates. For the rotary drum design, the field can be expressed in cylindrical coordinates (r, ϕ, z) relative to the drum axis [15]¹

$$\begin{aligned} B_r^a &= \sum_{n=0}^{\infty} b_n (r/R_{\text{drum}})^{-(2n+1)k-1} \\ &\quad \times \sin[(2n+1)k(\phi - \omega_{\text{drum}} t)] \\ B_\phi^a &= \sum_{n=0}^{\infty} -b_n (r/R_{\text{drum}})^{-(2n+1)k-1} \\ &\quad \times \cos[(2n+1)k(\phi - \omega_{\text{drum}} t)]. \end{aligned}$$

Actually, this approximation corresponds to an infinitely long drum with k symmetric pairs of North–South magnets, revolving with angular velocity ω_{drum} . For a particular design, the Fourier coefficients b_n can be obtained by measuring one of the field components B_r^a or B_ϕ^a at regular intervals along a perimeter $r = R_{\text{drum}}$. Usually, two or three coefficients will do.

B. Field Observed by Particle

As a particle moves through a magnetic field, it experiences a change of size and orientation of the field due to its own translational and rotational motion as well as through the

¹ Solutions of $\Delta A = 0$ of this kind can be found in [15].

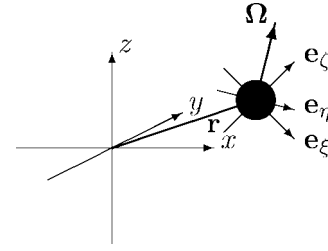


Fig. 2. Relation between lab frame and particle frame. The coordinate transformation matrix is $\mathbf{U} = (\mathbf{e}_\xi, \mathbf{e}_\eta, \mathbf{e}_\zeta)$.

inherent time-dependence of the field. If we neglect spatial variations of \mathbf{B}^a on the scale of the particle dimensions, we can define a magnetic field vector $\mathcal{B}^a(t)$ as the applied field experienced by the particle in its own coordinate frame: a frame that is rigidly connected to the particle.² Let $\mathbf{U}(t)$ be the coordinate transformation matrix between the particle frame and the lab frame, the columns of which are the unit vectors along the three axes of the particle coordinate system as expressed in the lab frame (see Fig. 2). Then $\mathcal{B}^a(t)$ is related to $\mathbf{B}^a(\mathbf{r}, t)$ by

$$\mathbf{U}(t) \cdot \mathcal{B}^a(t) = \mathbf{B}^a(\mathbf{r}(t), t)$$

and the variation of \mathcal{B}^a and \mathbf{U} with time is given by (see Appendix)

$$\begin{aligned} \mathbf{U} \cdot \frac{d}{dt} \mathcal{B}^a &= \frac{\partial}{\partial t} \mathbf{B}^a + (\mathbf{u} \cdot \nabla) \mathbf{B}^a - \boldsymbol{\Omega} \times \mathbf{B}^a \\ \frac{d}{dt} \mathbf{U} &= \boldsymbol{\Omega} \times \mathbf{U}. \end{aligned} \quad (3)$$

Here $\mathbf{r}(t)$ is the position of the particle and $\mathbf{u} = (d/dt)\mathbf{r}$ and $\boldsymbol{\Omega}$ are its translational and angular velocities. Note that the term $(d/dt)\mathbf{U} \cdot \mathcal{B}^a = \boldsymbol{\Omega} \times \mathbf{B}^a$ has been transferred to the right-hand side.

C. Particle Magnetic Moment

It was proposed in [12] and [13] that the magnetic moment of a nonferrous particle in a time-dependent field be described by an approximate evolution equation of the following form:

$$\frac{d}{dt} \mathcal{M} = -\mathcal{C} \cdot \mathcal{M} - \mathcal{D} \cdot \frac{d}{dt} \mathcal{B}^a. \quad (4)$$

The \mathcal{C} and \mathcal{D} tensors in this approximation will depend on the size, shape, and conductivity of the particle. Values for \mathcal{C} and \mathcal{D} can be calculated for simple particle shapes by fitting to the case of an harmonic field $\mathcal{B}^a(t) = \mathcal{B}_\omega^a e^{i\omega t}$. For example, for a cylindrical particle of radius R and length $L \gg R$ with its axis parallel to the z -axis in an harmonic field of frequency ω and arbitrary orientation, the magnetic moment is given by

$$\mathcal{M}(t) = \mathcal{M}_\omega e^{i\omega t}; \quad \mathcal{M}_\omega = \mathcal{N}_\omega \cdot \mathcal{B}_\omega^a \quad (5)$$

with

$$\mathcal{N}_\omega = \frac{\pi R^2 L}{\mu_0} \frac{J_2(i^{3/2} \sqrt{\mu_0 \omega \sigma R^2})}{J_0(i^{3/2} \sqrt{\mu_0 \omega \sigma R^2})} \begin{pmatrix} 2 & 0 & 0 \\ 0 & 2 & 0 \\ 0 & 0 & 1 \end{pmatrix} \quad (6)$$

² We will keep to script letters for vector quantities relative to the coordinate frame in which the particle is translationally and rotationally at rest and use the corresponding Roman bold type for the same quantities relative to the laboratory frame.

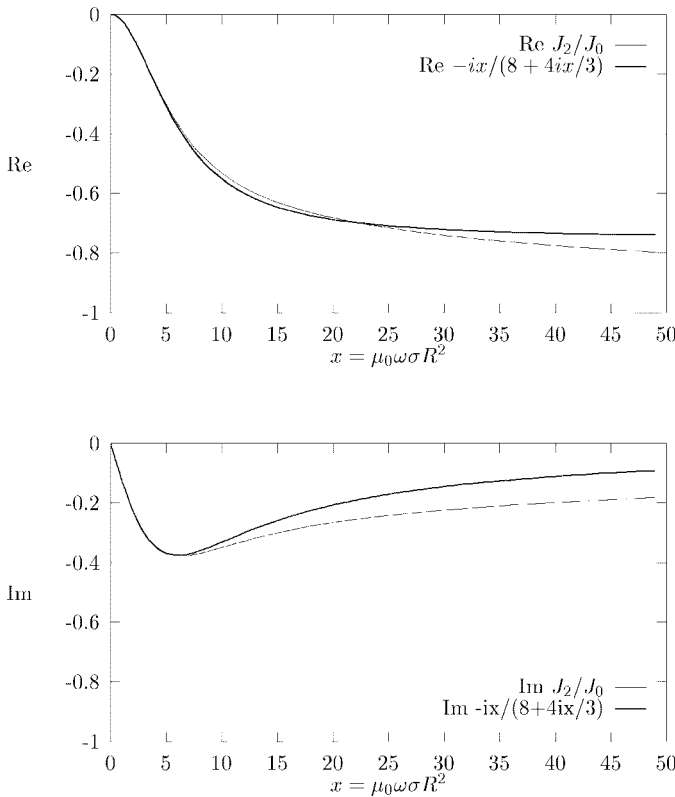


Fig. 3. Real and imaginary parts of the frequency-dependent part of the exact solution for \mathcal{N}_ω (thin lines) versus the rational function of $\mu_0\omega\sigma R^2$ (thick lines) resulting from the approximate (4).

where J_0 and J_2 are Bessel functions of order 0 and 2, respectively. In [13] the tensors \mathcal{C} and \mathcal{D} were fitted by substituting (5) into (4) and requiring the resulting expression for \mathcal{N}_ω to match the exact solution (6) for $|\mu_0\omega\sigma R^2| \ll 1$ and for $|\mu_0\omega\sigma R^2| = \infty$. However, in practice only the regime $|\mu_0\omega\sigma R^2| < 10$ is interesting, and it was found that a substantial improvement is obtained by fitting the degrees of freedom to match the second derivative of the real part and the first derivative of the imaginary part of \mathcal{N}_ω (see Fig. 3)

$$\mathcal{C} = \frac{6}{\mu_0\sigma R^2}$$

$$\mathcal{D} = \frac{3\pi R^2 L}{4\mu_0} \begin{pmatrix} 2 & 0 & 0 \\ 0 & 2 & 0 \\ 0 & 0 & 1 \end{pmatrix}.$$

In fact, with these choices, the agreement between simulation and experiment came close to the experimental error.

D. Mechanical Interactions

A fair share of the work of simulating a rotary drum eddy current separator goes into modeling the support and frictional forces between the particles and the conveyor belt, in spite of the fact that these are not the principal forces for the separation. In order to keep the model as simple as possible, the particles and the belt were allowed only three modes of contact: *roll*, *slide*, and *fly*. The shape of the particles was represented by an ellipsoid in order to avoid multiple points of contact between the particle and the belt.

For the *roll* mode it was assumed that the velocities of the particle and the belt match at the point of contact. This constraint defines the force of interaction between the belt and the particle, more in particular, the support force F^\perp and the friction force \mathbf{F}^{fric} . The transition between rolling and sliding was defined by the usual criterion

$$|\mathbf{F}^{\text{fric}}| > f^s F^\perp$$

with f^s the coefficient of static friction.

In the *slide* mode, the component of the particle velocity that is normal to the surface of the belt is kept to zero. In addition to this constraint the force of friction is modeled by

$$\mathbf{F}^{\text{fric}} = f^d F^\perp \frac{\Delta \mathbf{u}}{|\Delta \mathbf{u}| + \epsilon}.$$

Here, f^d is the dynamic friction factor, $\Delta \mathbf{u}$ is the differential velocity between the belt and the particle at their point of contact, and ϵ is a very small velocity constant guaranteeing the smoothness of the relation for numerical purposes. The transition from sliding to flying was defined by the criterion $F^\perp < 0$.

The usual particle trajectory is from rolling through sliding to flying (see Fig. 4). However, it was found that in one or two out of ten simulations involving flat particles, the particles sweep the belt shortly after losing contact. Also, at low belt speeds, light particles have a tendency to jump up and then collide with the belt after traveling a substantial distance through the air (see Fig. 4, bottom graph). In order to be able to simulate these cases, the model by Keller [16], [17] was used to compute the transfer of momentum during a collision. Keller's model is an elegant three-dimensional and energy-consistent formulation of inelastic collisions of rigid bodies, in which all the inelastic effects are combined in a single coefficient of restitution e : the ratio of the post- and pre-impact normal particle velocities. In our study, e was taken as a constant, independent of the size, shape, impact, velocity, or orientation of the particle. Such a simplification can be defended on the basis of a study by Stoianovici *et al.* [18] who showed that the rigid body theory performs remarkably well as long as little of the energy is absorbed by the system as longitudinal vibrations of the particle. They explicitly verified that the assumption of Coulomb's law of dry friction, which is essential to Keller's theory, is satisfied for impact velocities of the order of a few meters per s and that the coefficient of restitution does not depend much on the particle size or the impact velocity. It was found in [18] that e may depend strongly on the orientation of the particle, but this was attributed to the excitation of longitudinal vibrations of the particle. In the case of a metal particle-belt collision, the energy is absorbed by the belt rather than by the particle and the energy is absorbed locally, near the impact, independently of the shape and orientation of the particle.

E. Aerodynamic Forces

For flat particles, also the aerodynamic forces of drag and lift were included in order to get a feeling for their relative importance. It was found that for 10 mm disk-shaped particles,

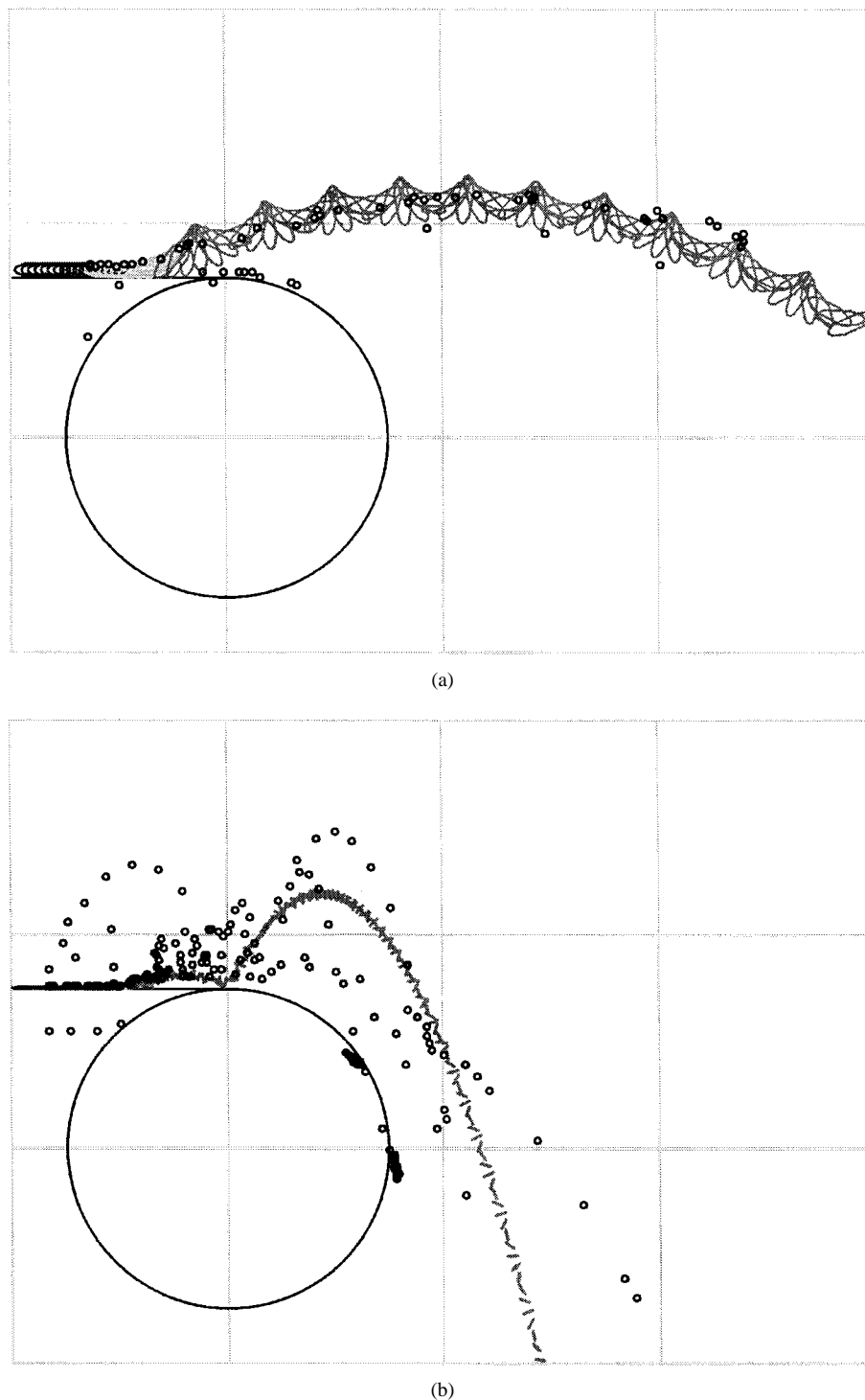


Fig. 4. (a) Usual particle trajectory is from rolling (black) through sliding (light grey) to flying (medium grey); operating conditions: belt speed 1.5 m/s, forward drum speed 35 rot/s, cylindrical aluminum particle of 15 mm diameter and 45 mm length. (b) For low belt speeds, particles may jump up early and fall down again; operating conditions: belt speed 0.5 m/s, forward drum speed 35 rot/s, disk-shaped aluminum particle of 10 mm diameter and 2 mm thick. Open circles define (X, Y) -positions recorded by a video camera for the operating conditions of the simulation.

trajectories, simulated with and without this contribution, would differ slightly (see Fig. 5).

III. EXPERIMENTAL VERIFICATION

The model was tested against a large number of experiments with a BM 29.701/18 industrial rotary drum separator and a

laboratory vertical disk separator [7] (see Table I for details of the machines).³ In the experiments, the particles were tracked with the help of a video camera and the resulting images were translated into a series of (X, Y) -coordinates by image

³The eddy current separator used for the experiments is model BM 29.701/18, from Bakker Magnetics, Son, The Netherlands.

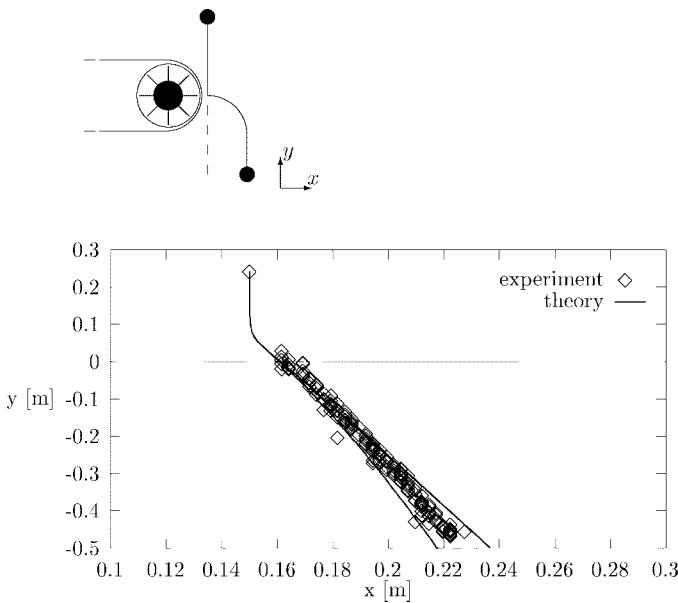


Fig. 5. Experimental and simulated trajectories are shown for copper disks of 10 mm diameter and 2 mm thickness deflected by a Bakker Magnetics BM 29.701/18 with a forward drum speed of 50 Hz. The disks are dropped close to the rotating magnetic drum of the eddy current separator as shown in the upper figure. The diamonds represent experimental data and the continuous lines show the results of simulations without (curve to the left) and including (curve to the right) aerodynamic forces.

TABLE I
MACHINE AND OPERATING PARAMETERS OF THE EXPERIMENTS

| Parameter | BM 29.701/18 | Laboratory vertical disk |
|-------------------------------------|------------------------|--------------------------|
| number of pairs of poles k | 9 | 6 |
| $R_{\text{belt/disk}}$ [mm] | 149 | 169 |
| gap between disks [mm] | | 50 |
| remnant field of magnets [T] | 1.13 | 0.73 |
| belt speed [m/s] | 0.5, 1.0, 1.5 | |
| $\omega_{\text{drum/disk}}$ [rad/s] | $40\pi, 70\pi, 100\pi$ | 55π |

processing.⁴ In order to get a comparison between experiment and theory, the equations of motion were integrated with the help of the differential-algebraic equation (DAE)-integrator DASSL [19], [20] for the conditions of the experiments. Table II defines the particles used in the experiments.

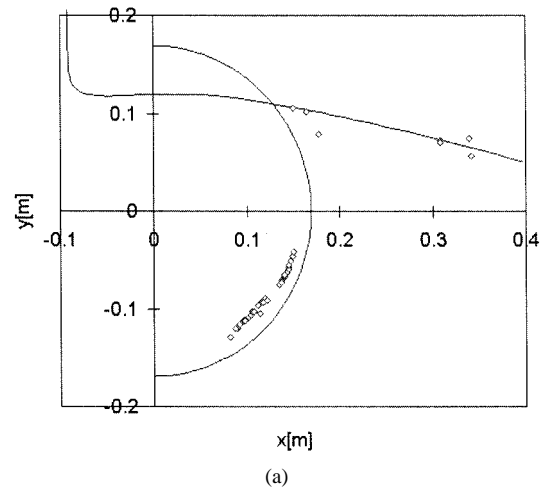
A. Vertical Disk Separator

Only a few isolated experiments were done on the laboratory vertical disk separator. Fig. 6 shows a comparison of experimental results and simulation for two particles. The disks prevent a view of the entire particle trajectory but the few data points that are available for the aluminum cylinder show that the simulation is within the range of experimental error. A similar comparison for the aluminum disk gives less accurate results. A third experiment with an aluminum sphere of 15 mm diameter (not presented here) shows a deviation with the corresponding simulation of the same magnitude as for the disk, but now with the other sign. From this, we conclude

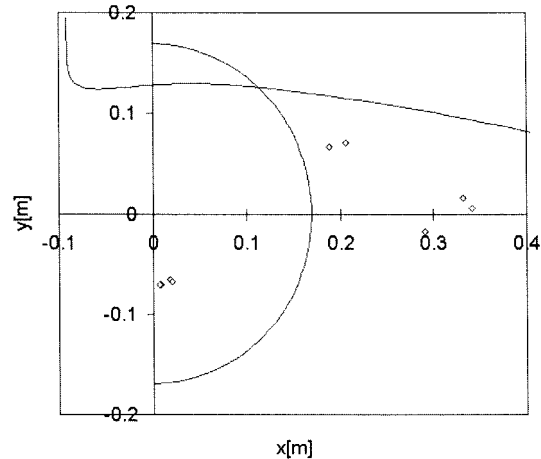
⁴Graphical software TimWin of Difa Measuring Systems B.V., Breda, The Netherlands.

TABLE II
PARTICLE SHAPES, SIZES, AND COMPOSITIONS USED IN THE EXPERIMENTS

| shape | material | diameter [m] | length/height [m] |
|----------|-----------|--------------|-------------------|
| sphere | aluminium | 0.010 | |
| sphere | aluminium | 0.018 | |
| cylinder | aluminium | 0.003 | 0.010 |
| cylinder | aluminium | 0.005 | 0.015 |
| cylinder | aluminium | 0.008 | 0.024 |
| cylinder | aluminium | 0.010 | 0.030 |
| cylinder | aluminium | 0.015 | 0.045 |
| cylinder | aluminium | 0.020 | 0.060 |
| cylinder | copper | 0.010 | 0.030 |
| cylinder | copper | 0.030 | 0.090 |
| disk | aluminium | 0.010 | 0.002 |
| disk | aluminium | 0.015 | 0.0024 |
| disk | aluminium | 0.020 | 0.0022 |
| disk | copper | 0.015 | 0.0031 |



(a)



(b)

Fig. 6. Examples of direct comparisons between experimental and simulated particle trajectories on the laboratory vertical disk separator. (a) Aluminum cylinder of 10 mm diameter and 30 mm length and (b) aluminum disk of 15 mm diameter and 2.4 mm height.

that the exact match of the cylinder case is fortuitous and the error in the angle of deflection is typically of the order of 10%.

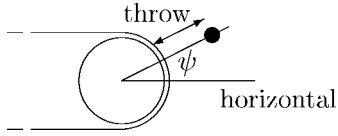


Fig. 7. Definition of the throw of a particle.

B. Rotary Drum Separator

All particles of Table II were processed on the rotary drum separator at nine different operating conditions, with belt speeds of 0.5 m/s, 1.0 m/s, and 1.5 m/s and forward drum speeds of 20 rot/s, 35 rot/s, and 50 rot/s. The belt speeds were chosen rather low with respect to belt speeds used in practice, which are typically 1–3 m/s, because of the limitations of the video camera which could take a maximum of 25 shots per s. Even at 1.5 m/s belt speed, particles had to be replaced up to ten times on the belt to get a sufficient number of particle positions to define a single trajectory.

The examples of particle trajectories shown in Fig. 4 are typical for the majority of the more than hundred cases that were compiled. The graphs show agreement of the general behavior of experiment and simulation, as with the vertical disk separator. At higher belt speeds collisions between the particles and the belt become less frequent, except for disk-shaped particles. Such particles have a tendency to be lifted from the belt by the contact force resulting from the magnetic torque, so that the lift disappears immediately after losing contact and the rotation makes them touch the belt in a sweeping motion. The trajectories of these particles are very much reproducible, despite the effects of the collision. In contrast, collisions at low belt speed, such as shown in the bottom graph of Fig. 4, lead to a multitude of different particle trajectories. The simulation realizes only one of these because there are no stochastic elements in the computation. However, slight variations of e.g., the friction coefficient have a large effect on the simulated tracks as would be expected.

C. Statistical Comparison

The results of experiment and simulation can also be compared statistically by plotting the simulated throw against the experimental throw. The throw was defined as the distance between the surface of the drum and the center of the particle at a predefined angle ψ between the radius vector of the particle and the horizontal (see Fig. 7). The data shown are for $\tan \psi = 0.5$.

In Fig. 8 the experimental and simulated throw are compared for a belt speed of 1.5 m/s. The data points correspond to 36 tracks of the 42 tracks that can be generated by processing the set of 14 particles from Table II at three different drum speeds. Cases containing a scatter of different experimental trajectories due to collisions were left out from the statistics.

The results show a standard deviation of about 14 mm and on average the simulations are 12 mm short of the experimental values. Both of these values seem independent of the throw itself. On average, the error in the prediction is around 10%.

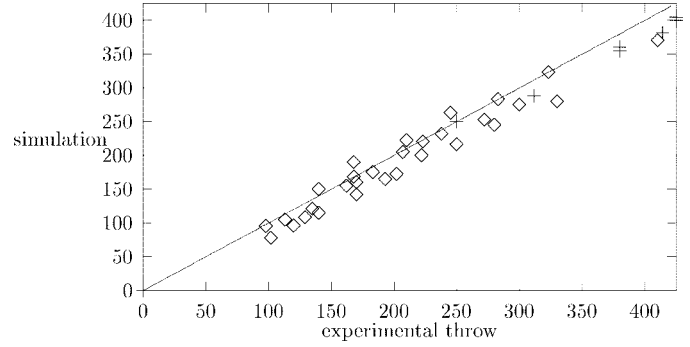


Fig. 8. Simulated throw versus experimental throw for all particles, drum speeds of 20 rot/s, 35 rot/s, and 50 rot/s and a belt speed of 1.5 m/s. The unit along either axis is 0.84 mm.

The wavelength of the BM 29.701/18 is about 105 mm. This means that particles larger than about 35 mm are outside the range covered by the dipole approximation. The data points in Fig. 8 corresponding to particles larger than 35 mm have been marked with a +. In general, there seems to be no clear deviation caused by the size of these particles contrary to theory. This may be due to the fact that only large cylinders have been tried and no large disk-shaped or spherical particles. The rather tolerant behavior of the model for larger cylinders is fortunate though because cylindrical particles tend to be the largest particles present in a given sieve fraction.

IV. CONCLUSION

The improved model for the magnetic force of eddy current separators on nonferrous particles can be used to predict particle throw with a relative error of about 10% at typical operating conditions. For rotary drum separators the simple mechanical models used to account for the contact and friction forces do not seem to degrade the accuracy very much, except perhaps for cases where the particle hits the belt after a substantial ballistic flight. In these latter cases, the simulation realizes one of the many possible experimental particle trajectories, but slight variations of the input parameters have a large effect on the simulation result.

APPENDIX

Equation (3) for the change of the separator magnetic field with time, as experienced by the particle, may be derived by taking the derivative of both sides of

$$\mathbf{U}(t) \cdot \mathcal{B}^a(t) = \mathcal{B}^a(\mathbf{r}(t), t)$$

with respect to time, so as to get

$$\frac{d}{dt} \mathbf{U} \cdot \mathcal{B}^a + \mathbf{U} \cdot \frac{d}{dt} \mathcal{B}^a = \frac{\partial}{\partial t} \mathcal{B}^a + \frac{\partial}{\partial r_i} \mathcal{B}^a \frac{dr_i}{dt}.$$

Transferring the first term on the left to the right-hand side, and using

$$\frac{d}{dt} \mathbf{U} \cdot \mathcal{B}^a = (\boldsymbol{\Omega} \times \mathbf{U}) \cdot \mathcal{B}^a = \boldsymbol{\Omega} \times (\mathbf{U} \cdot \mathcal{B}^a) = \boldsymbol{\Omega} \times \mathcal{B}^a$$

relation (3) is obtained.

ACKNOWLEDGMENT

The authors are grateful to D. Bongers for simulating the experiments on the vertical disk separator.

REFERENCES

- [1] W. L. Dalmijn, "Practical applications of eddy currents in the scrap recycling," in *Proc. 2nd Int. Symp. Recycling Metals Eng. Mater., Minerals, Metals & Mat. Soc.*, 1990, pp. 303–314.
- [2] T. A. Edison, U.S. Patent 400 317, 1889.
- [3] E. Schlömann, "Separation of nonmagnetic metals from solid waste by permanent magnets. I. Theory," *J. Appl. Phys.*, vol. 46, no. 11, pp. 5012–5021, 1975.
- [4] E. Schlömann, "Separation of nonmagnetic metals from solid waste by permanent magnets II. Experiments on circular disks," *J. Appl. Phys.*, vol. 46, no. 11, pp. 5011–5029, 1975.
- [5] H. J. L. van der Valk, W. L. Dalmijn, and W. P. C. Duyvesteyn, *Erzmetall*, vol. 41, pp. 266–274, 1988.
- [6] H. J. L. van der Valk, B. C. Braam, and W. L. Dalmijn, "Eddy-current separation by permanent magnets Part I: Theory," *Resources Conservation*, vol. 12, p. 233–252, 1986.
- [7] B. C. Braam, H. J. L. van der Valk, and W. L. Dalmijn, "Eddy-current separation by permanent magnets Part II: Rotating disc separators," *Resources, Conservation, Recycling*, vol. 1, pp. 3–17, 1988.
- [8] R. Meier-Staude and A. Mersmann, "Analytic modeling of particle trajectories by eddy current separation," *Schüttgut*, vol. 3, pp. 307–311, 1997.
- [9] D. Fletcher, R. Gerber, P. Lawson, and J. Boehm, "Eddy current separation of nonferrous conductors and nonconductors: Theory and initial experiments," *IEEE Trans. Magn.*, vol. 27, pp. 5375–5377, Nov. 1991.
- [10] D. Fletcher, R. Gerber, L. Tarrant, and T. Reid, "Experimental validation and generalized theory of a single boundary eddy-current separator model," *IEEE Trans. Magn.*, vol. 28, pp. 2415–2417, Sept. 1992.
- [11] D. Fletcher and R. Gerber, "Electromagnetic separation: The prediction and measurement of conductor separability," *IEEE Trans. Magn.*, vol. 29, pp. 3255–3257, Nov. 1993.
- [12] P. A. Leest, P. C. Rem, and W. L. Dalmijn, "Analytical approach for custom designing of eddy current separators," in *Proc. XLVI. Berg- und Hüttenmännischer Tag*, Freiberg, Germany, 1995, pp. 1–8.
- [13] P. C. Rem, P. A. Leest, and A. J. van den Akker, "A model for eddy current separation," *Int. J. Min. Proc.*, vol. 49, pp. 193–200, 1997.
- [14] E. g., L. D. Landau and E. M. Lifshitz, *Electrodynamics of Continuous Media*. London, U.K.: Pergamon, 1963, p. 143.
- [15] M. R. Spiegel, "Fourier analysis," in *Schaum's Outline Series*. New York: McGraw-Hill, 1974, p. 39.
- [16] J. B. Keller, "Impact with friction," *J. Appl. Phys.*, vol. 53, pp. 1–4, 1986.
- [17] Y. Wang and M. T. Mason, "Two-dimensional rigid-body collisions with friction," *J. Appl. Phys.*, vol. 59, pp. 635–642, 1992.
- [18] D. Stoianovici and Y. Hurmuzlu, "A critical study of the applicability of rigid-body collision theory," *J. Appl. Phys.*, vol. 63, pp. 307–316, 1996.
- [19] L. R. Petzold, "A description of DASSL: Differential algebraic system solver," Sandia National Laboratories, Livermore, CA, SAND82-8637, Sept. 1982.
- [20] K. E. Brenan, S. L. Campbell, and L. R. Petzold, "Numerical solution of initial value problems," in *Differential-Algebraic Equations*. New York: Elsevier, 1989.